frontiers in Earth Science

ORIGINAL RESEARCH
published: 16 March 2021
doi: 10.3389/feart.2021.637056

Development and Interplay of Two Orthogonal Fault Systems in the NW Qaidam Basin, Northern Tibetan Plateau

Kai Huang[1,2], *Lei Wu*[1,2]*, *Haifeng Zhao*[1,2], *Junyong Zhang*[3], *Yongshu Zhang*[4], *Ancheng Xiao*[1], *Yan Chen*[4] *and Hanlin Chen*[1,2]

[1]*Key Laboratory of Geoscience Big Data and Deep Resource of Zhejiang Province, School of Earth Sciences, Zhejiang University, Hangzhou, China,* [2]*Research Center for Structures in Oil and Gas Bearing Basins, Ministry of Education, Hangzhou, China,* [3]*Bureau of Geophysical Prospecting Inc., China National Petroleum Corporation, Zhuozhou, China,* [4]*Research Institute of Exploration and Development, Qinghai Oilfield Company, PetroChina, Dunhuang, China*

OPEN ACCESS

Edited by:
Renqi Lu,
China Earthquake Administration, China

Reviewed by:
Hong Chang,
Chinese Academy of Sciences, China
Yangwen Pei,
China University of Petroleum (Huadong), China

***Correspondence:**
Lei Wu
leiwu@zju.edu.cn

Specialty section:
This article was submitted to Structural Geology and Tectonics, a section of the journal Frontiers in Earth Science

Received: *02 December 2020*
Accepted: *08 February 2021*
Published: *16 March 2021*

Citation:
Huang K, Wu L, Zhao H, Zhang J, Zhang Y, Xiao A, Chen Y and Chen H (2021) Development and Interplay of Two Orthogonal Fault Systems in the NW Qaidam Basin, Northern Tibetan Plateau. Front. Earth Sci. 9:637056. doi: 10.3389/feart.2021.637056

How fold and thrust belts (FTBs) evolve over time and space in a transpressional regime remains poorly understood. Based on high-resolution 3D seismic reflection data and remote sensing images, we herein present a detailed structural analysis of the Cenozoic faults in the NW margin of the Qaidam Basin that is bounded to the north by the left-reverse Altyn Tagh fault system. Two sets of orthogonal, basement-involved faults with contrasting geometries, kinematics, and temporal development are identified. One set consists of generally E-W-striking, N-dipping, reverse faults with a component of sinistral shear. They are parallel or subparallel to the Altyn Tagh fault system, led to southward tilting of the basement, and formed a local unconformity between the middle Miocene Shangyoushashan formation and underlying strata. They developed in an out-of-sequence order, and were mostly active during 43.8–15.3 Ma but in relatively tectonic quiescence with limited weak reactivation since then. The second set is mainly composed of the NNW-striking reverse faults with dextral shear components. They are approximately perpendicular to the Altyn Tagh fault system, and intensively active since ~15.3 Ma, much later than the initiation of the E-W-striking faults. Together with published results, we ascribe the development of these two sets of orthogonal faults as the transition from transpression to left lateral slip on the central segment of the Altyn Tagh fault system. The two fault sets interplayed with each other in two ways: 1) the older E-W-striking faults were offset by younger NNW-striking faults, and 2) the younger NNW-striking faults curved to link with the preexisting E-W-striking faults. Our findings reveal that transpressional-dominated FTBs evolve in a more complicated way than the contractional-dominated ones, and more site-based case studies are needed to reveal the underlying primary principles.

Keywords: 3-D seismic reflection data, Altyn Tagh fault system, transpression, fault interplay, growth strata

INTRODUCTION

Fold and thrust belts (FTBs) are common features in basin margins under contractional regime (e.g., Jia, 2005; Morley et al., 2011; Lacombe and Bellahsen, 2016; Cheng et al., 2017), and sensitive to the tectonic activity of bordering orogenic belts and/or large-scale reverse faults. Numerous prior studies have been conducted in most of typical FTBs on the Earth and other terrestrial planets like Mars and Titan (e.g., Liu et al., 2016; Klimczak et al., 2018; Herrero Gil et al., 2020). They have provided a first-order image of geometries and kinematics of FTBs, and further, the way and underlying mechanisms of the deformation propagation from orogenic belts to adjacent basins. FTBs may also develop in a transpressional regime, and are commonly characterized by development of faults with various geometries and kinematics. These different sets of faults may interplay with each other when the FTBs evolve, resulting in more complicated deformation patterns than those under a contractional regime. This issue, however, has not yet been fully addressed.

Sandwiched between the left-slip Altyn Tagh Fault (ATF) and the East Kunlun Fault (EKF) to the northwest and south, respectively (**Figure 1**), the Qaidam Basin is the largest sedimentary basin inside the Tibetan Plateau in the Cenozoic, and provides an ideal field laboratory to understand the structural deformation pattern of FTBs in a transpressinal regime. Two sets of mutually orthogonal fault systems have been reported in the northwestern margin of the Qaidam Basin, which is also known as the Altyn slope in the southern side of the ATF (Zhao et al., 2016). One set is E-W-striking, and usually regarded as branch faults of the ATF; whereas the other is NW-NNW-striking, and forms the numerous folds that could be easily observed in the field and remote sensing images (Mao et al., 2016). Whilst the E-W-striking faults are generally left-reverse (Wu et al., 2019), the NW-NNW-striking ones are thought to be either right-reverse (Mao et al., 2016; Huang et al., 2018) or left-reverse (Du et al., 2019a; Liu et al., 2019). The activity time of these two sets of faults systems is also highly disputed. Wu et al. (2019) elucidated that the E-W-striking faults were active prior to ~15 Ma, predating the development of NW-NNW-striking faults since the middle Miocene. On the contrary, Du et al. (2019a) inferred that the NW-NNW-striking structures initiated in the Oligocene, a bit earlier than the formation of the E-W-striking faults. Moreover, the interplay between these two sets of fault systems remains unassessed. In this contribution, we apply high-resolution 3D seismic reflection data in Dongping area in the NW Qaidam Basin, together with surface geology revealed by remote sensing images, to study the geometries, kinematics, activity time, and interplay of these two sets of fault systems. Our findings bear implications for the evolution of FTBs in transpressional regimes, and regionally, for the growth mechanism of the northern Tibetan Plateau.

GEOLOGICAL SETTING

Lying within the northern margin of the Tibetan Plateau at an average elevation of ~2, 800 m and covering an area of

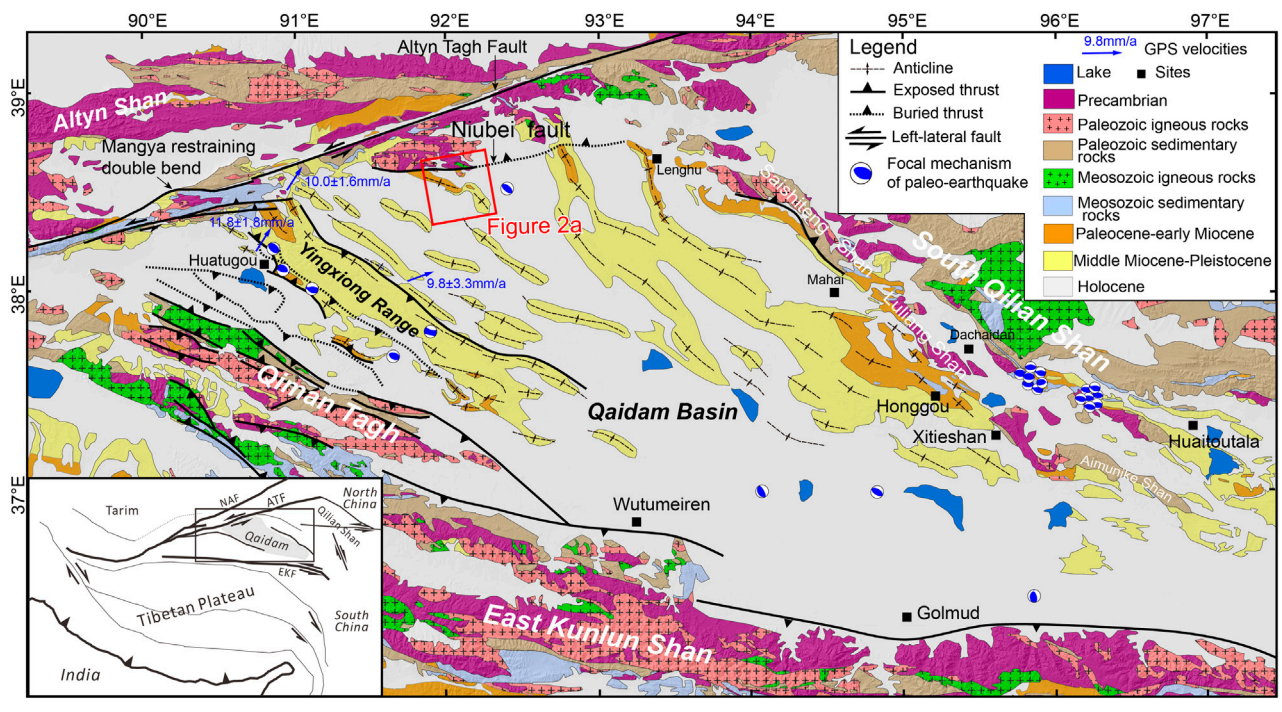

FIGURE 1 | Simplified geological map of the Qaidam Basin and adjacent areas, modified from Wei et al. (2016). Its location is shown in the inset tectonic map of the Tibetan Plateau in the lower-left corner. ATF, Altyn Tagh Fault; EKF, East Kunlun Fault; WK, West Kunlun Mountain; NAF, North Altyn Tagh Fault.

120,000 km^2, the Qaidam Basin is a rhomb-shaped intermountain basin bounded by the Altyn Tagh fault system to the northwest, the South Qilian Shan thrust belt to the northeast, and the East Kunlun fault system to the south (**Figure 1**). The depocenters of the Qaidam Basin resides approximately along its central axis during most of the Cenozoic era, and is gradually migrating eastward over time, implying that it likely formed as a synclinorium (Bally et al., 1986; Meng and Fang, 2008) rather than a foreland basin (Yin et al., 2002; Zhu et al., 2006; Cheng et al., 2019). Reconstruction of basin development based on regional or local 2D/3D seismic data revealed that, whilst the Qaidam Basin has been undergoing shortening since the early Paleogene, intense deformation that generates the numerous NW-striking anticlinal belts within the basin (**Figure 1**) occurred as late as the late Miocene (Zhou et al., 2006; Xiao et al., 2013; Wu et al., 2014; Wei et al., 2016). Two models have been proposed to account for the driving mechanism underlying the formation of these anticlinal belts in the western Qaidam Basin. The convergence model is characterized by the Qaidam Basin moving parallelly or slightly obliquely to the ATF, inducing NE-SW-directed crustal shortening with limited dextral shear component (Mao et al., 2016; Huang et al., 2020). This model is consistent with GPS observations (Gan et al., 2007). The block rotation model predicts ~10° clockwise rotation of the Qaidam Basin that facilitates NW-WNW-striking sinistral transpressional shear along the anticlinal belts (Liu et al., 2019). This model, however, is inconsistent with the GPS and paleomagnetic measurements indicating minimal rotation of the Qaidam Basin in the Cenozoic (Dupont-Nivet et al., 2002; Gan et al., 2007; Yu et al., 2014).

The Cenozoic deposits within the Qaidam Basin are mainly terrestrial clastic rocks with a maximum thickness over 15 km. From old to young, they are subdivided into eight formations (**Table 1**): the Lulehe Fm (LLH), Lower Xiaganchaigou Fm (LXG), Upper Xiaganchaigou Fm (UXG), Shangganchaigou Fm (SG), Xiayoushashan Fm (XY), Shangyoushashan Fm (SY), Shizigou Fm (SZG), Qigequan Fm (QGQ). Although absolute ages of these formations have been determined by paleomagnetostratigraphic studies of many sedimentary sections cross the basin (Yang et al., 1997; Sun et al., 2005; Fang et al., 2007; Gao et al., 2009; Lu and Xiong, 2009; Zhang et al., 2013; Wang et al., 2017; Nie et al., 2019), they are not consistent with each other due to lack of reliable radiometric or biostratigraphic constraints, and fall into two contrasting age models (Wu et al., 2019). The relatively old age model, in which the bottom of the Cenozoic strata is assigned as Early Eocene, is adopted in this study (**Table 1**), as suggested by Wu et al. (2019).

TABLE 1 | Cenozoic stratigraphy of the Qaidam Basin. Modified from Wu et al. (2019) and Huang et al. (2020).

Formations	Symbols	Basal ages (Ma)
Qigequan	QGQ	2.5
Shizhigou	SZG	8.1
Shangyoushashan	SY	15.3
Xiayoushashan	XY	23.0
Shangganchaigou	SG	35.5
Upper Xiaganchaigou	UXG	41.5
Lower Xiaganchaigou	LXG	43.8
Lulehe	LLH	53.5

Surface Geology of the Study Region

Our study region is situated in the middle of the northwestern margin of the Qaidam Basin, and in the junction area between the NW-NNW-striking structures in the basin interior and the E-W-striking structures adjacent to the ATF (**Figure 1**). Therefore, this is an ideal place to evaluate the development and interplay of these nearly orthogonal fault systems.

Three major anticlines have developed in this region (**Figure 2A**). The first is the NNW-striking South Dongping anticline that is characterized by a series of NW-striking, right-stepping, en echelon minor folds at surface, indicating a certain degree of NNW-striking dextral shear (**Figure 2B**). Quaternary QGQ Fm is outcropped in the core of the anticline. The second is the E-W-striking Dongping anticline to the north. Late Eocene–Oligocene SG Fm is well exposed in the core of this anticline, and deformed by a left-stepping, en echelon array of ESE-striking secondary anticlines, as well as some minor NE-striking left-lateral and NNW-striking right-lateral faults (Wu et al., 2019) (**Figure 2C**). These secondary structures together suggest a component of E-W-striking sinistral shear along the Dongping anticline (**Figure 2C**). The third is the NW-striking Hongsanhan anticline in the northwest of the study region. This anticline is a superimposed buckle fold (Du et al., 2019b), and highly asymmetric with a wide southwestern limb and a very narrow northeastern limb (**Figure 2A**). LLH to XY Fms are well exposed in the anticline. Faults controlling the formation of these anticlines are nearly invisible in the field, because of covering of late Quaternary alluvial deposits and saline mudstone deposited in playas.

A large E-W-striking fault, the Niubei fault, is existent in the north of our study region, and linked with the ATF to the west (**Figures 1**, **2A**). It was a syn-depositional sinistral transpressional fault in ~53.5–17 Ma, followed by intense reverse faulting during 17–15 Ma and tectonic quiescence since ~15 Ma (Wu et al., 2019). This pattern was regarded as a response to the tectonic reorganization of the Altyn Tagh fault system in the middle Miocene (Wu et al., 2019).

SEISMIC DATA AND METHODS

We applied 3D seismic reflection data to reveal the subsurface structures in the study area. These data cover an area of approximately 500 km^2 and involve the Dongping anticline, the South Dongping anticline and the eastern part of the Hongsanhan anticlines. They are pre-stack processed with the two-way travel time (TWTT) up to 5 s and spatial resolution of ~100 m. Geological interpretations, including faults and stratigraphic boundaries, were conducted in the seismic data based on calibration of borehole loggings and surface geology. Along-layer similarity attributes (also known as coherency) on

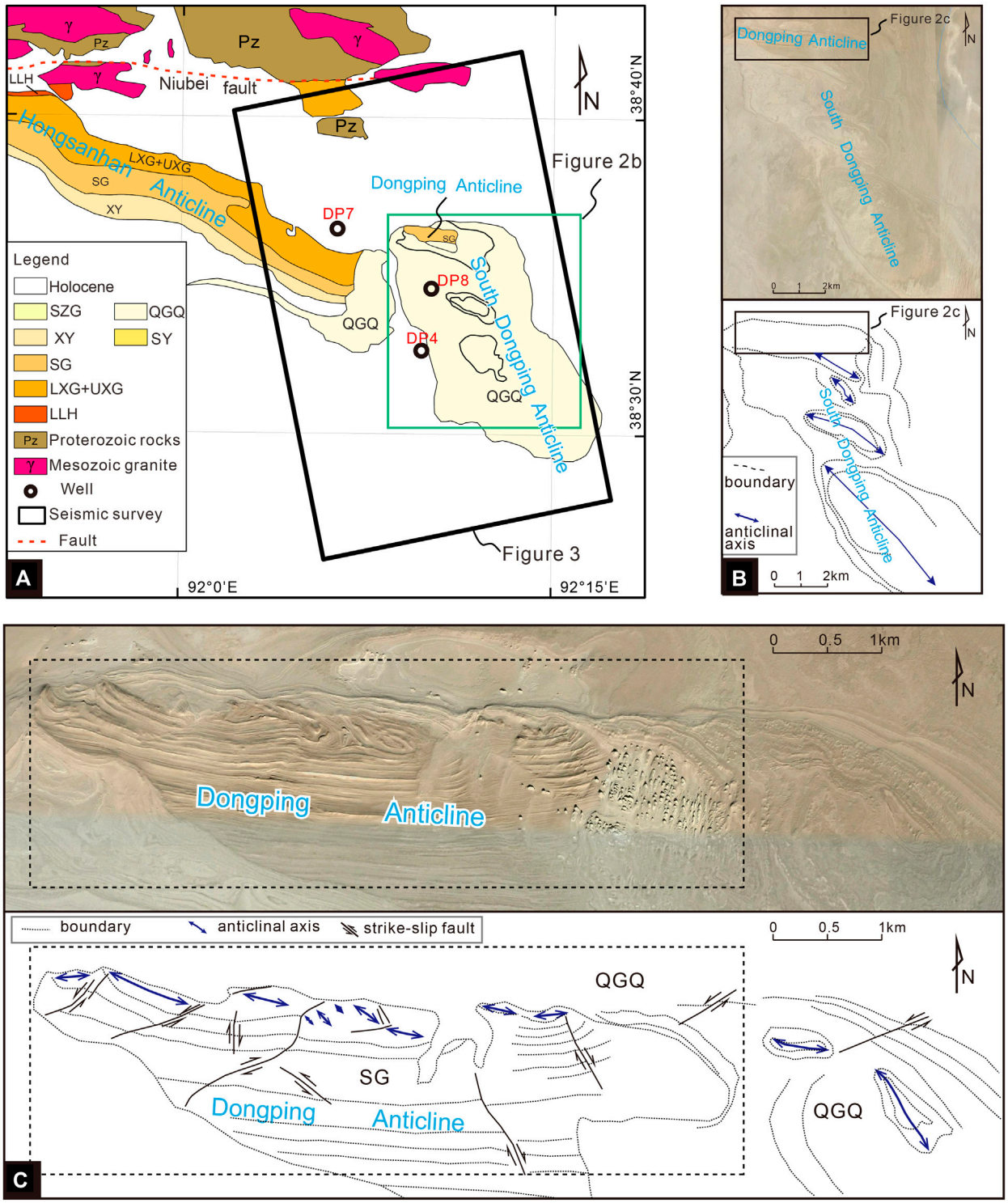

FIGURE 2 | (A) Geological map of Dongping area. **(B)** Remote sensing images showing surface deformation: a group of NNW-oriented dextral transpressional anticlines in the south and an E-W-striking sinistral transpressional belt in the north. **(C)** Zoom-in of the sinistral transpressional belt, showing a series of en echelon anticlines and minor strike-slip faults. The interpretation within the dotted rectangle is modified from Wu et al. (2019). Abbreviations for the Cenozoic units are same as those in **Table 1**.

the bottom of the LLH and SG Fms (**Figures 3A,B**) were extracted from the 3-D seismic volume by applying the semblance algorithm that highlights lateral amplitude variations between adjacent seismic traces (Bahorich and Farmer, 1995). These coherency maps were used to assist in understanding the fault distribution in map view. Activity time of each fault was determined by identifying related growth strata, and associated fault throw and throw rate during the deposition period of each stratigraphic unit was quantified by calculating the thickness difference between both sides of the fault.

FAULT GEOMETRIES AND RELATED GROWTH STRATA

We recognized two major groups of basement-involved reverse faults that are nearly orthogonal to each other (**Figure 3C**). One is approximately E-W-striking (e.g., F2n, F3, F4, F5e, F6e, F8, F9, F10), and the other is NNW- to NW-striking (e.g., F1, F2s, F5w, F6w, F7). Some additional thin-skinned NW-striking reverse faults were also observed between Fault F1s and F2s. These basement-involved faults are described in detail in this study as follows. Six composite seismic reflection sections, which

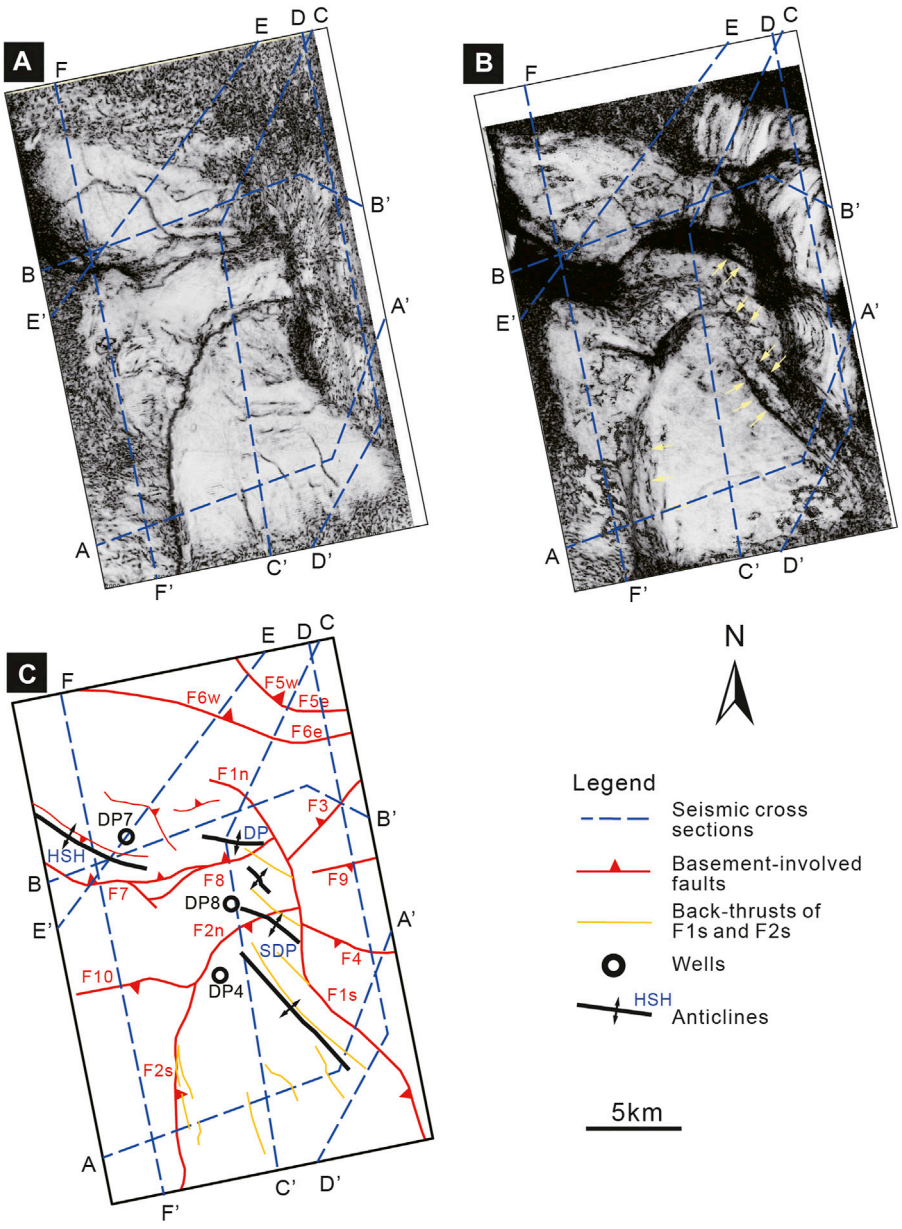

FIGURE 3 | (A) Along-layer coherent slice of the bottom of Lulehe formation (LLH). **(B)** Along-layer coherent slice of the bottom of Shangganchaigou formation (SG), yellow arrows mark the thin-skinned reverse faults that are generally oblique to F1s and F2s with <45° angles. **(C)** Fault systems projected to the base of Lulehe formation (LLH) in map view. HSH, Hongsanhan anticline; DP, Dongping anticline; SDP, South Dongping anticline.

traverse the above-mentioned major faults, are presented with geological interpretations to elucidate the geometries of the studied fault groups (**Figures 3C**, **4**, and **5**, and **Table 2**).

E-W-Striking Basement-Involved Faults

Fault F5e and F6e are N-dipping basement-involved thrust faults lying in the northernmost of our seismic survey, and connect with the larger E-W-striking Niubei fault to the north through NW-striking F5w and F6w (**Figure 3C**). They cut and folded the pre-Cenozoic basement and LLH–XY Fms, resulting in the southward tilting of the basement and the development of a local angular unconformity between the SY Fm and underlying strata (**Figure 5A**). This unconformity gradually changes to conformable contact toward the basin interior. Strata above the unconformity are only slightly deformed. Growth strata consisting of LXG to SZG Fms are observed in the hanging wall of F6e, with the best occurring in the XY Fm.

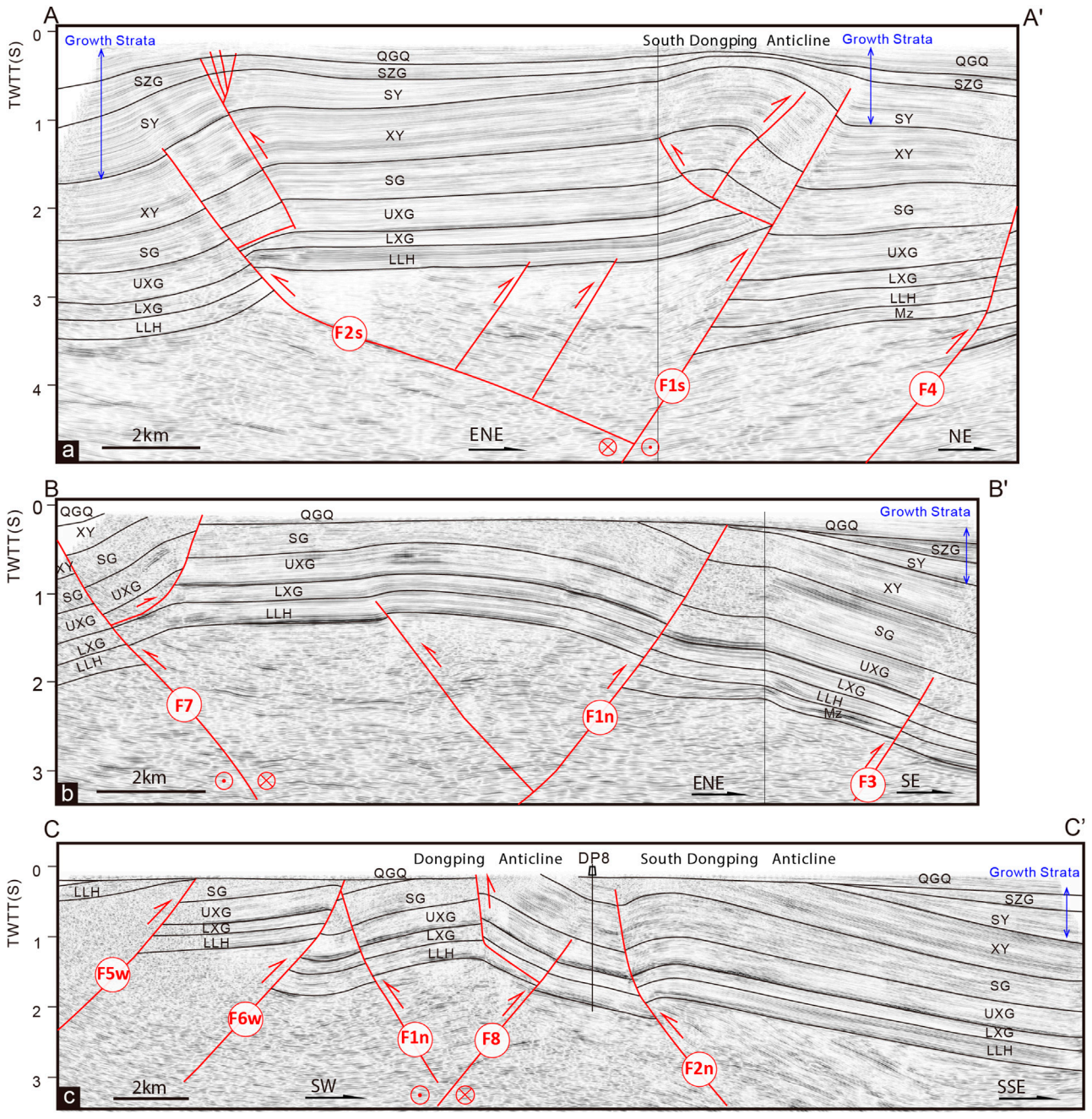

FIGURE 4 | Three seismic reflection sections across major faults in the study region. The location is shown in **Figure 3**. Mz represents the Mesozoic (mainly Middle Jurassic). Abbreviations for the Cenozoic units are same as those in **Table 1**. TWTT, Two-way travel time.

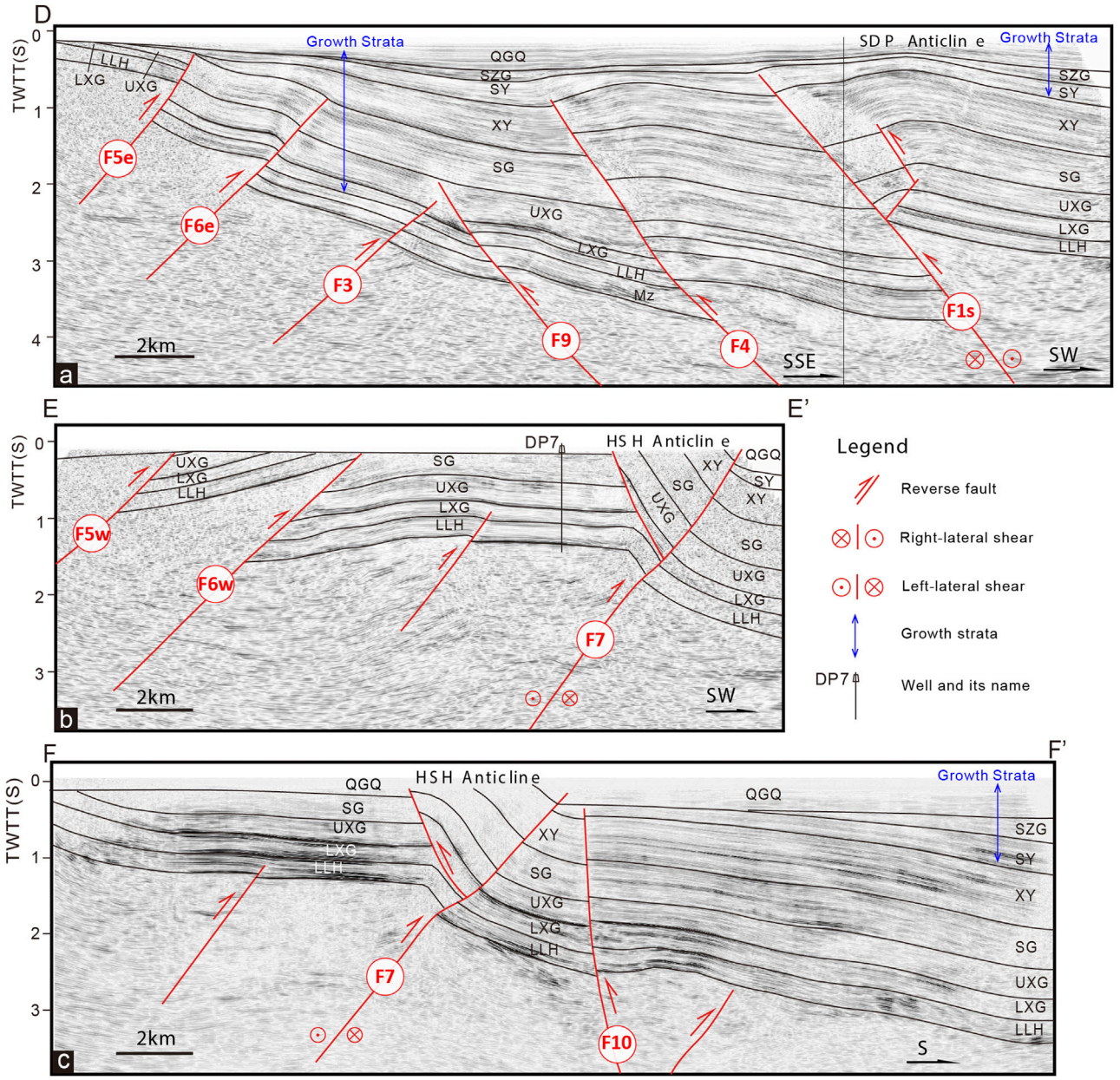

FIGURE 5 | Three additional seismic reflection sections across major faults in the study region. The location is shown in **Figure 3**. Abbreviations are same as those in **Figure 4**.

The N-dipping F8 is a steep basement-involved fault to the southwest of F6e. It cuts the basement upward into the UXG Fm, resulting in the occurrence of growth strata, though unapparent, in the UXG Fm that is overlain conformably by the non-growth SG Fm (**Figure 4C**). Together with the northern end of F1n, F8 controls the shape of the Dongping anticline, with a back-thrust developing in the hanging wall and soling in the mudstone in the LLH Fm. According to the consistency between deformed UXG-XY Fms, which is unconformably overlain by horizontal QGQ Fm atop F8, and the overlying syn-tectonical SY-SZG Fms to the south (**Figure 4C**), we interpret that F8 should be also active during the deposition periods of SY and SZG Fms. F8 extends against the F1 toward east (**Figure 3C**). Fault F3 has similar geometry to F8, and is located on the other side of F1. It slightly deformed the LLH–UXG Fms, with the appearance of growth strata in the UXG Fm (**Figure 5A**).

Fault F9 is another basement-involved fault in the footwall of F1 and located to the south of F3 (**Figure 5A**). It dips to the south, and cuts the basement upward into the UXG Fm, with the development of growth strata in the UXG Fm overlain conformably by non-growth SG Fm.

TABLE 2 | Summary of growth strata and activity time of faults in the study region.

Fault name		Growth strata and associated sections[a]	Activity time (Ma)[b]
NWN- to NW-striking	F1n	SY-QGQ (B-B′)	<15.3–0
	F1s	SY-QGQ (A-A′)	15.3–0
	F2s	SY-QGQ (A-A′)	15.3–0
	F5w, F6w[c]	Between SG and QGQ (C-C′, E-E′)	<15.3–2.5
	F7	SY-QGQ (E-E′, F-F′)	<15.3–0
Approximately E-W-striking	F2n	XY-SZG (C-C′)	23–2.5
	F3	UXG (D-D′)	41.5–35.5
	F4	XY-SZG (D-D′)	23–2.5
	F5e, F6e	LXG-SZG (D-D′)	43.8–2.5
	F8	UXG, SY - SZG (C-C′)	41.5–35.5, <15.3–2.5
	F9	UXG (D-D′)	41.5–41.5
	F10	LXG, SY-SZG (F-F′)	43.8–41.5, <15.3–2.5

[a]*Detailed description of growth strata related to a specific fault is presented in the main text.*
[b]*Activity time is determined by the age of growth strata according to the time framework in* ***Table 1****.*
[c]*Growth strata of these two faults are not indirectly observed in seismic sections, but could be loosely constrained by underlying pre-growth strata (LLH-SG Fms) and overlying horizontal QGQ Fm.*

The S-dipping (60–70°) fault F10 is located to the southwest of F8 and linked with F2s and F2n to the east (**Figure 3C**). It cuts through the basement rocks up to the SZG Fm, resulting in thinning of LXG and SY-SZG Fms in the hanging wall (**Figure 5C**). To the east, the S-dipping basement-involved F2n cuts and folds the LLH–SZG Fm in the hanging wall, forming a secondary anticline of the larger South Dongping anticline (**Figure 3C**). Obvious F2n-related growth strata are observed in the SY and SZG Fms that are unconformably overlain by the weakly deformed QGQ Fm (**Figure 5C**). Whilst minimal thickness change has been detected in the XY Fm, we still attribute it as growth strata comparing with the underlying SG Fm that thickens toward F2n. F2n lies against the N-S-striking F1 to the east. Fault F4 with similar characteristic of F2n develops on the other side of F1. It cuts and folds the LLH–SZG Fms that are unconformably overlain by the nearly horizontal QGQ Fm, with well-developed growth strata in the SY and SZG Fms but inapparent growth strata in the XY Fm (**Figure 5A**).

NNW- to NW-Striking Basement-Involved Faults

Fault F1s (also termed Pingdong Fault) strikes approximately NNW in map view (**Figure 3C**). It dips ~50–70° toward west, cuts the basement rocks upwards into the SY Fm, forming the South Dongping anticline in the hanging wall (**Figure 4A**). This fault is one of the major faults in western Qaidam Basin, because it has accumulated more than one thousand meters of basement uplift, and controls the distribution of the Mesozoic strata. Drilling data reveal that Mesozoic (mainly Middle Jurassic) strata are only preserved in the footwall of F1s, but missing in the hanging wall, indicating that it was likely a preexisting reverse fault prior to the Cenozoic. Growth strata related to F1s are clearly observed in the SY and SZG Fm that are unconformably overlain by less deformed Qigequan (QGQ) Fm (**Figure 4A**). Some NE-dipping back-thrusts develop in the hanging wall of F1s, and sole into the LXG and LLH Fms. They are en echelon right-stepping distributed in the map view (**Figure 3C**), indicating a component of dextral shear of F1s. Fault F1n is the northward continuation of F1s to the north of F8, and disappears further north. It does not have as much displacement as F1s, and together with fault F8, controls the shape of Dongping anticline. Growth strata are not observed in the LLH–XY Fms in the hanging wall, and the overlying SY and SZG Fms, which are overlain by horizontal QGQ Fm, are missing on top of F1n (**Figure 4C**).

The approximately N-S-striking fault F2s is located to the south of F2n and F10 (**Figure 3C**). It dips steeply to the east, and extends from the basement upward into the SY Fm (**Figure 4A**). F2s forms the western boundary fault of the box-shaped South Dongping anticline, which is characterized by a nearly wide and horizontal core but narrow and steep limbs. Some thin-skinned, SW-dipping back-thrusts, which are in en echelon right-stepping arrangement, develop in its hanging wall, indicating a certain component of dextral shear on F2s. Growth strata related to F2s occur in the SY -QGQ Fms.

The NW-striking F5w and F6w dip toward the NE, and cut upward from the basement to the SG Fm that is well exposed at surface or unconformable overlain by the QGQ Fm (**Figures 4C**, **5B**). Pre-Cenozoic basement in the hanging walls tilts toward north, different from that of the conterminous F5e and F6e to the east (**Figures 3C**, **5B**). Growth strata are not well developed in the remaining LLH–SG Fms in the hanging walls of F5w and F6w (**Figure 4C**).

The NW-striking, NE-dipping F7 is a steep basement-involved fault to the southwest of F6w, elevating the basement in the hanging wall to be hundreds of meters higher than that in the footwall (**Figures 4B**, **5B**,C). A SW-dipping back-thrust develops on top of F7, constituting a flower structure indicative of strike-slip shear. LLH–SY Fms have been intensely deformed in the hanging wall of this back-thrust, forming the Hongsanhan anticline at surface. Growth strata are not observed in the LLH–XY Fms in the southern limb of the Hongsanhan anticline (**Figures 4B**, **5B**). F7 likely connects the basement-involved E-W-striking fault F8 to the east.

INTERPRETATION

Fault Kinematics

Whilst all presented faults in our study region are reverse in section view, strike-slip shear is expected to have occur on these faults based on following observations. First, they are in the vicinity of the left-reverse Altyn Tagh fault system. Second, they are all high-angle basement-involved faults and form many flower or half-flower structures. Third, present-day GPS velocity in the western Qaidam Basin is generally NE-directed (Wang et al., 2017; Wang and Shen, 2020; **Figure 1**), oblique to their strikes. And fourth, strata in the hanging walls of F1s and F2s, which are cut by some secondary faults, are not balanced across faults in 2-D profiles (**Figure 4A**). The E-W-striking Dongping anticline, which is controlled by fault F8, consists of a set of en echelon distributed, ESE-striking secondary anticlines, as well as some minor NE-striking left-lateral and NNW-striking right-lateral faults (**Figure 2C**), suggesting a component of sinistral shear on F8. This is consistent with the kinematics of the larger E-W-striking Niubei fault to the north, which has been testified as a left-reverse fault (Wu et al., 2019). The NNW-striking South Dongping anticline bounded by F1s and F2s to the west and east, respectively, however, features a series of NW-striking, right-stepping, en echelon minor folds at surface (**Figure 2B**) and secondary faults at depth (**Figure 3C**), indicating dextral shear on F1s and F2s.

Fault Development Over Time

Based on the above descriptions of fault-related growth strata, we interpreted activity time of these faults and thus delineated the spatial and temporal patterns of fault development in our study region. The results are listed in **Table 2** and **Figure 6**, and reveal different deformation patterns of the two orthogonal fault systems. The E-W-striking faults were generally initiated during the deposition periods of the LXG–XY Fms (43.8–15.3 Ma) in an out-of-sequence order, but most of them ceased their activity prior to the deposition of SY Fm (~15.3 Ma) with limited weak reactivations. Activity of the NW- to NNW-striking faults, however, generally commenced in the deposition period of SY Fm (~15.3–8.1 Ma), much later than that of the E-W-striking faults, and continue to the present. We further calculated the intensity of fault activity over time by measuring the fault throw of each period. The result (**Figure 7**) reveals that the E-W-striking faults were intensely active during the deposition periods of UXG (41.5–35.5 Ma) and XY (23–15.3 Ma) Fms, but became weakly active, or even inactive in the deposition period of SY–QGQ Fm (<15.3 Ma), when intense activity on the NNW-striking faults happened.

DISCUSSION

Formation Mechanisms of the Two Fault Systems

The above analyses and interpretations reveal two orthogonal basement-involved reverse fault systems that contrast in geometries, kinematics, and temporal development in the NW margin of the Qaidam Basin. The E-W-striking faults are generally N-dipping, oblique to the ATF, and left-reverse. They result in southward tilting of the basement and form a local unconformity between the SY Fm and underlying strata (**Figure 5A**). They were intensively active prior to the deposition of SY Fm (~15.3 Ma), but in a state of tectonic quiescence with limited weak reactivtions henceforth (**Figure 7**). This deformation pattern, which has been reported by Wu et al. (2019), is only observed in the NW margin of the Qaidam Basin and has never been found elsewhere. It is thus reasonable to attribute the development of these E-W-striking faults to the tectonic movement of the Altyn Tagh fault system that bounds the Qaidam Basin to the northwest. The NNW- to NW-striking faults are approximately perpendicular to the Altyn Tagh fault system, and form under right-laterally transpressional setting during the deposition periods of SY Fm (**Figure 7**), much later than the initiation of the E-W-striking faults. These deformation characteristics are similar to the NW- to NNW-striking faults that dominate the first-order tectonic framework in the interior of the modern Qaidam Basin (Mao et al., 2016).

Taken the deformation features of these two fault systems together, our findings reveal a change of structural deformation from E-W-striking sinistrally transpressional faulting to NNW- to NW-striking right-laterally transpressional faulting in the middle Miocene in the NW margin of the Qaidam Basin. This change was likely attributed to the middle Miocene reorganization of the Altyn Tagh fault system, as previously proposed by Wu et al. (2019). Specifically, the present-day active central segment of the ATF may not form during the deposition periods of LLH to XY Fms. The North Altyn Fault and the Jinyanshan Fault to the north defined the northwestern boundary of the Qaidam Basin, constituting a large restraining bend on the eastern termination of the Altyn Tagh fault system at the time (Wu et al., 2019; **Figure 8A**). The E-W-striking faults formed in this left-reverse transpressional restraining bend. The central segment of the ATF started to form in the late deposition period of the XY Fm (~17 Ma), cutting through the restraining bend (Wu et al., 2019). The strike-slip efficiency of the ATF was very low in its initial stage due to lack of smooth fault traces. In this scenario, deformation along the ATF was dominated by vertical uplift rather than horizontal displacement, as attested by physical analog (Hatem et al., 2017), resulting in intense reverse faulting on the E-W-striking faults that formed the local angular unconformity below the SY Fm. The present ATF was finally established at ca. 15.3 Ma when it completely cut through the bend and the E-W-striking faults in the NW Qaidam Basin (Wu et al., 2019). Left-slip strain was then largely localized on the ATF, resulting in an abrupt decrease in the intensity of tectonic activity of the E-W-striking faults. Fast slip on the ATF was absorbed by NE-SW-directed crustal shortening over the entire northern Tibetan Plateau (Zhang et al., 2007; Zheng et al., 2013), which triggered the widely distributed NNW- to NW-striking reverse faulting in the Qaidam Basin. As the NNW- to NW-striking faults are oblique to the regional maximum principle stress (σ_1) and lie against the sinistral ATF with a large angle, a component of dextral shear is manifested.

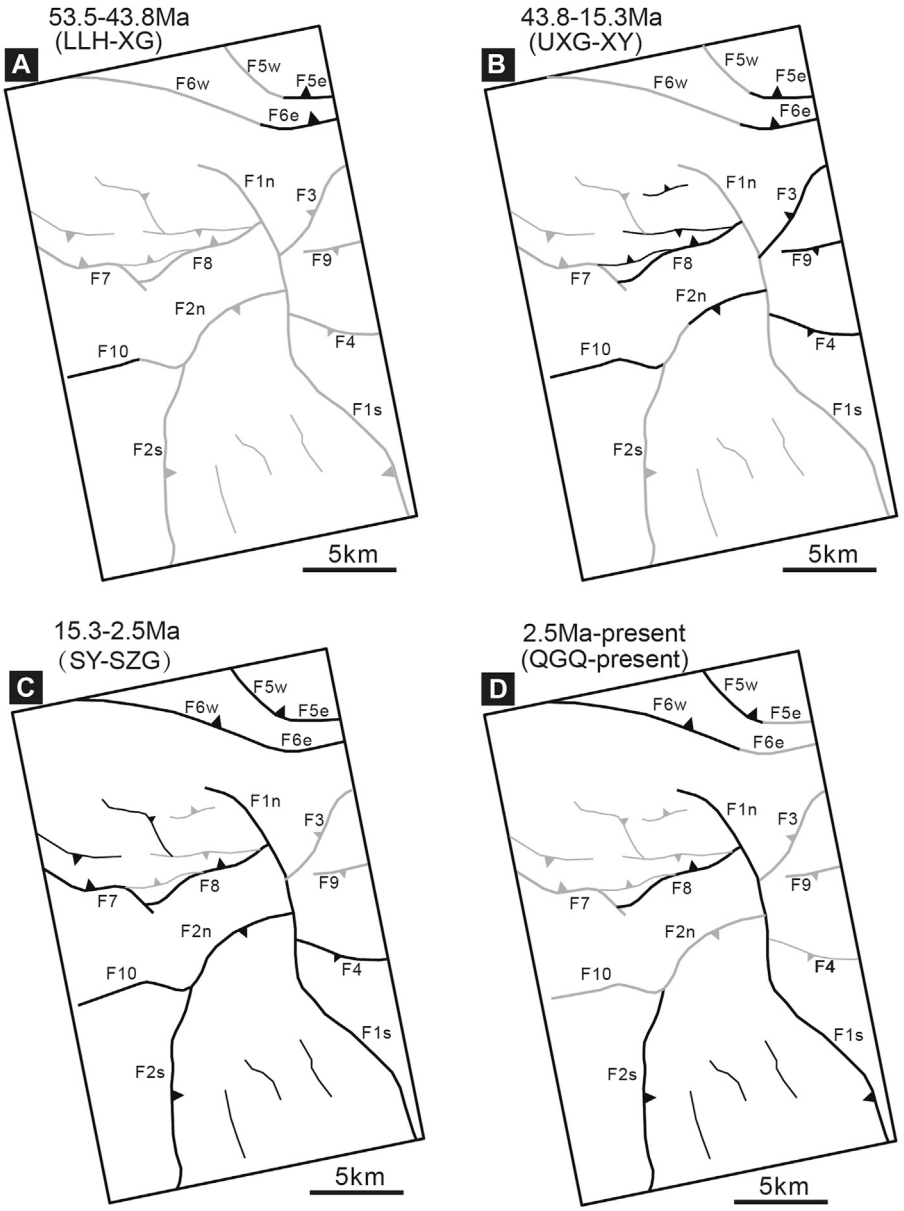

FIGURE 6 | Summary of temporal development of the basement-involved faults within the study area. Black solid lines are active faults during corresponding period; whereas gray lines represent inactive ones.

Interplay Between the Two Fault Systems and Implication for the Development of Transpressional-Dominated FTBs

As the two orthogonal fault systems spatially overlap, we observe two aspects of interplay between them.

First, the relatively older E-W-striking faults were offset by younger NNW-striking faults. Specifically, F8 and F3 are two E-W-striking, N-dipping basement-involved faults in the western and eastern sides of the NNW-striking F1, respectively. They both extend from the basement upward into the UXG Fm, resulting in slight thinning of the UXG Fm in its hanging wall. We interpret that these two faults were likely active and linked to each during the deposition period of UXG Fm, but became tectonically inactive in the subsequent deposition periods of SG and XY Fms. Right-laterally transpressional fault F1 was initiated since the deposition period of SY Fm (~15.3 Ma), offsetting F8 and F3, and resulting in reactivation of F8 in its hanging wall. Similarly, F2n and F4 are two E-W-striking, S-dipping basement-involved faults in the western and eastern sides of the F1, respectively. Analysis of associated growth strata indicates that they both became active since the deposition of XY Fm (~23 Ma). Similar geometries, kinematics, activity time and spatial coincidence imply that they were possibly linked to each other

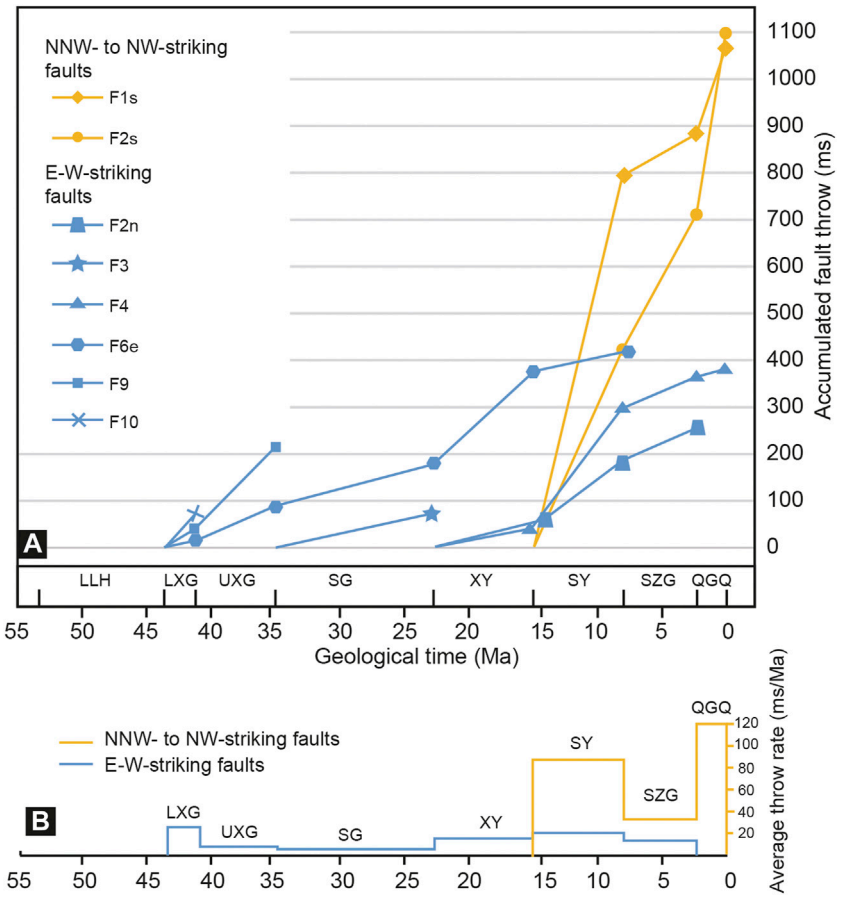

FIGURE 7 | Plot of accumulated throws **(A)** and throw rate **(B)** of the basement-involved faults vs. geological time, showing the contrasting temporal development of E-W-striking and NNW- to NW-striking faults.

prior to the deposition of SY Fm (~15.3 Ma), but were offset right-laterally by F1 since then. If our above correlations are correct, ~2 km right-lateral offset is predicted on F1 since ~15.3 Ma.

Second, the younger NNW-striking faults curved to link with the preexisting E-W-striking faults. This is well documented by the N-S-striking F2s, which curves toward the east to link with the E-W-striking F2n to the northeast. Similar situation also occurred on NW-striking F5w and F6w, which curve on their southeastern ends to connect with F5e and F6e, respectively. This common pattern indicates that preexisting faults may result in lateral heterogeneity of rocks involved in the deformation, and thus change the local stress field to generate complex fault geometries.

Our findings bear meaningful implications for the development of FTB in a transpressional setting. Typical contractional-dominated FTBs are usually characterized by long-distance, thin-skinned over-thrusting and expands from hinterland to inland with increasing width over time, following the critical wedge taper theory (Dahlen et al., 1984; Suppe, 2007), such as those in the nearby SW and N margins of the Tarim Basin (Li et al., 2012; Cheng et al., 2017). However, in a transpressional-dominated FTB, faults are usually high-angle to facilitate vertical uplift and lateral offset rather than horizontal shortening, and the width of fault zone may abruptly decrease in response to strain localization on the neighboring boundary transpressional fault (Frost et al., 2009; Zhao et al., 2016; Wu et al., 2019), such as the tectonic quiescence of the E-W-striking faults since ~15.3 Ma. Moreover, faults with contrasting geometries, kinematics, and activity time, like the E-W-striking and NNW- to NW-striking faults in this study, could develop in different time and space due possible to highly-heterogeneous stress field in a transpressional-dominated FTB. These different faults may interplay with each other to generate very complex fault systems. In brief summary, transpressional-dominated FTBs evolve in a more complicated way than the contractional-dominated ones, with highly spatio-temporal heterogeneity in fault development. More site-based case studies should be conducted to obtain the underlying primary principles, possibly in combined use of surface geology, subsurface geophysical data as well as physical analog and/or numerical modeling.

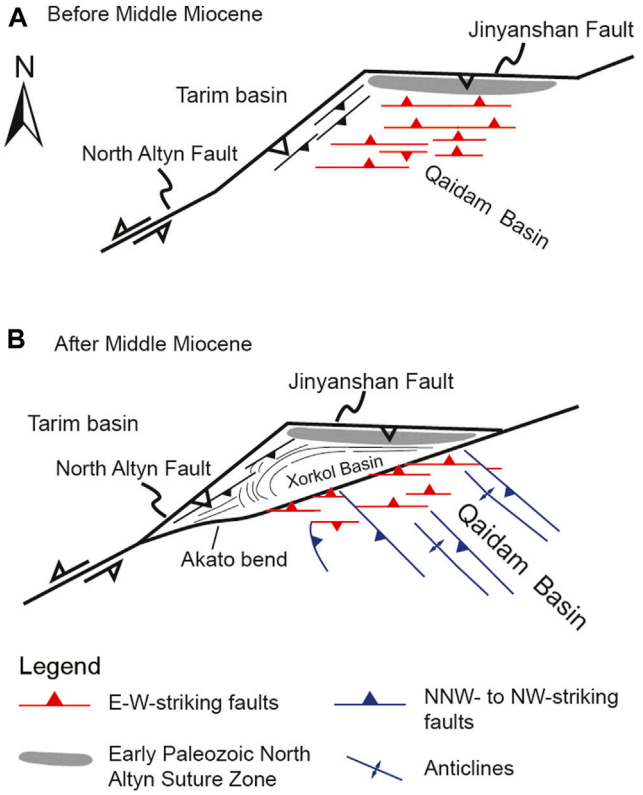

FIGURE 8 | Diagrams illustrating the possible genetic relationships between the two fault systems and the bordering Altyn Tagh fault system. Modified from Wu et al. (2019). Lineation in the Altyn Shan modified from Wang et al., 2008.

CONCLUSION

Based on 3D seismic reflection data and remote sensing images, we herein reveal two groups of high-angle basement-involved transpressional faults (E-W-striking and NNW- to NW-striking, respectively) that contrast in geometries, kinematics, and temporal development in the Dongping area, NW Qaidam Basin. The E-W-striking faults are parallel or subparallel to the bordering Altyn Tagh fault system. They dip generally to the N with a component of sinistral shear, resulting in southward tilting of the basement and a local unconformity between the SY Fm and underlying strata. They were mainly active during the deposition period of LXG to XY Fms (43.8–15.3 Ma), but almost ceased their activities since then. The NNW- to NW-striking faults, however, are characterized by a component of dextral shear and intense activity since ~15.3 Ma. Our results thus suggest a significant structural reorganization in the NW Qaidam Basin, likely associated with the tectonic evolution of the bordering Altyn Tagh fault system. We further observed close interplay between these two orthogonal fault systems, implying that transpressional-dominated FTBs have very complicated evolutional processes than ever thought.

DATA AVAILABILITY STATEMENT

The original contributions presented in the study are included in the article/Supplementary Material, further inquiries can be directed to the corresponding author.

AUTHOR CONTRIBUTIONS

The idea was provided by the corresponding author LW. First author KH mainly accomplished the manuscript together with LW and HZ. Seismic data and divided layers were offered by JZ and YZ. The other authors gave much advice for this manuscript. All authors agree to be accountable for the content of the work.

FUNDING

This study is funded by National Natural Science Foundation of China (41972218, 41402170), the Fundamental Research Funds for the Central Universities (2019QNA3013), and Research Institute of exploration and development, Qinghai Oilfield Company, PetroChina.

ACKNOWLEDGMENTS

We appreciate the seismic data provided by the Qinghai Oil Company.

REFERENCES

Bahorich, M., and Farmer, S. (1995). 3-D seismic discontinuity for faults and stratigraphic features: the coherence cube. *The Leading Edge* 14, 1053–1058. doi:10.1190/1.1437077

Bally, A. W., Chou, I., Clayton, R., Eugster, H. P., Kidwell, S., Meckel, L. D., et al. (1986). *Notes on sedimentary basins in China; report of the American sedimentary basins delegation to the people's Republic of China*. US: US Geological Survey, 86–327.

Cheng, F., Garzione, C. N., Jolivet, M., Guo, Z., Zhang, D., Zhang, C., et al. (2019). Initial deformation of the northern Tibetan plateau: insights from deposition of the Lulehe formation in the Qaidam Basin. *Tectonics* 38, 741–766. doi:10.1029/2018TC005214

Cheng, X., Chen, H., Lin, X., Wu, L., and Gong, J. (2017). Geometry and kinematic evolution of the hotan-tiklik segment of the western Kunlun thrust belt: constrained by structural analyses and apatite fission track thermochronology. *J. Geol.* 125, 65–82. doi:10.1086/689187

Dahlen, F. A., Suppe, J., and Davis, D. (1984). Mechanics of fold-and-thrust belts and accretionary wedges Cohesive Coulomb theory. *J. Geophys. Res. Solid Earth* 89, 10087–10101. doi:10.1029/JB089iB12p10087

Du, W., Chen, Y., Wang, Z., Bian, Q., and Guo, Z. (2019a). Tectonic analysis and petroleum significance of Cenozoic faults in Dongping-Niuzhong area in Altyn slope. *Pet. Exploration Dev.* 46, 983–990. doi:10.1016/S1876-3804(19)60254-5

Du, W., Zhang, D., Yu, X., Cheng, X., Wang, Z., Bian, Q., et al. (2019b). Relationship between the Altyn Tagh strike-slip fault and the Qaidam Basin : New insights from superposed buckle folding in Hongsanhan : New

insights from superposed buckle folding in Hongsanhan. *Int. Geol. Rev.* 62, 1570–1580. doi:10.1080/00206814.2019.1661039

Dupont-Nivet, G., Butler, R. F., Yin, A., and Chen, X. (2002). Paleomagnetism indicates no neogene rotation of the Qaidam Basin in northern tibet during indo-asian collision. *Geology* 30, 263. doi:10.1130/0091-7613(2002)030<0263:PINNRO>2.0.CO;2

Fang, X., Zhang, W., Meng, Q., Gao, J., Wang, X., King, J., et al. (2007). High-resolution magnetostratigraphy of the neogene huaitoutala section in the eastern Qaidam Basin on the NE Tibetan plateau, Qinghai province, China and its implication on tectonic uplift of the NE Tibetan plateau. *Earth Planet. Sci. Lett.* 258, 293–306. doi:10.1016/j.epsl.2007.03.042

Frost, E., Dolan, J., Sammis, C., Hacker, B., Cole, J., and Ratschbacher, L. (2009). Progressive strain localization in a major strike-slip fault exhumed from midseismogenic depths: structural observations from the Salzach-Ennstal-Mariazell-Puchberg fault system, Austria. *J. Geophys. Res.* 114 (B4), B04406. doi:10.1029/2008JB005763

Gan, W., Zhang, P., Shen, Z.-K., Niu, Z., Wang, M., Wan, Y., et al. (2007). Present-day crustal motion within the Tibetan Plateau inferred from GPS measurements. *J. Geophys. Res.* 112 (B8), B08416. doi:10.1029/2005JB004120

Gao, J. P., Sheng-Xi, L. I., Dai, S., Ai-Yin, L. I., and Peng, Y. H. (2009). Constraints of tectonic evolution in provenance from detrital zircon fission-track data of Cenozoic strata of Xichagou district in western Qaidam Basin. *J. Lanzhou Univ.* 45, 1–7. doi:10.13885/j.issn.0455-2059.2009.03.012 [in Chinese with English abstract]

Hatem, A. E., Cooke, M. L., and Toeneboehn, K. (2017). Strain localization and evolving kinematic efficiency of initiating strike-slip faults within wet kaolin experiments. *J. Struct. Geology.* 101, 96–108. doi:10.1016/j.jsg.2017.06.011

Herrero Gil, A., Ruiz, J., and Romeo, I. (2020). Lithospheric contraction on Mars: a 3D model of the amenthes thrust fault system. *J. Geophys. Res. Planets* 125, ee2019JE006201. doi:10.1029/2019JE006201

Huang, K., Chen, L., Xiao, A., Shen, Y., and Wu, L. (2018). Cenozoic deformation characteristics of the xianshuiquan anticline in the northwestern Qaidam Basin and its significance. *Geol. J. China Universities* 24 (5), 761–768. doi:10.16108/j.issn1006-7493.2018012 [in Chinese with English abstract]

Huang, K., Wu, L., Zhang, J., Zhang, Y., Xiao, A., Lin, X., et al. (2020). Structural coupling between the Qiman Tagh and the Qaidam Basin, northern Tibetan Plateau: a perspective from the Yingxiong Range by integrating field mapping, seismic imaging, and analogue modeling. *Tectonics* 39, e2020TC006287. doi:10.1029/2020TC006287

Jia, C. Z. (2005). Foreland thrust-fold belt features and gas accumulation in Midwest China. *Petrol. Explor. Dev.* 32 (4), 9–15. [in Chinese with English abstract]

Klimczak, C., Kling, C. L., and Byrne, P. K. (2018). Topographic expressions of large thrust faults on Mars. *J. Geophys. Res. Planets* 123, 1973–1995. doi:10.1029/2017JE005448

Lacombe, O., and Bellahsen, N. (2016). Thick-skinned tectonics and basement-involved fold-thrust belts: insights from selected Cenozoic orogens. *Geol. Mag.* 153, 763–810. doi:10.1017/S0016756816000078

Li, S., Wang, X., and Suppe, J. (2012). Compressional salt tectonics and synkinematic strata of the western Kuqa foreland basin, southern Tian Shan, China. *Basin Res.* 24, 475–497. doi:10.1111/j.1365-2117.2011.00531.x

Liu, R., Chen, Y., Yu, X., Du, W., Cheng, X., and Guo, Z. (2019). An analysis of distributed strike-slip shear deformation of the Qaidam Basin, northern Tibetan plateau. *Geophys. Res. Lett.* 46, 4202–4211. doi:10.1029/2018GL081523

Liu, Z. Y. C., Radebaugh, J., Harris, R. A., Christiansen, E. H., and Rupper, S. (2016). Role of fluids in the tectonic evolution of Titan. *Icarus* 270, 2–13. doi:10.1016/j.icarus.2016.02.016

Lu, H., and Xiong, S. (2009). Magnetostratigraphy of the dahonggou section, northern Qaidam Basin and its bearing on cenozoic tectonic evolution of the qilian Shan and Altyn Tagh fault. *Earth Planet. Sci. Lett.* 288, 539–550. doi:10.1016/j.epsl.2009.10.016

Mao, L., Xiao, A., Zhang, H., Wu, Z., Wang, L., Shen, Y., et al. (2016). Structural deformation pattern within the NW Qaidam Basin in the Cenozoic era and its tectonic implications. *Tectonophysics* 687, 78–93. doi:10.1016/j.tecto.2016.09.008

Meng, Q., and Fang, X. (2008). Cenozoic tectonic development of the Qaidam Basin in the northeastern Tibetan plateau. *The Geol. Soc. America* 120, 1–24. doi:10.1130/2008.2444(01

Morley, C. K., King, R., Hillis, R., Tingay, M., and Backe, G. (2011). Deepwater fold and thrust belt classification, tectonics, structure and hydrocarbon prospectivity: a review. *Earth-Science Rev.* 104, 41–91. doi:10.1016/j.earscirev.2010.09.010

Nie, J., Ren, X., Saylor, J. E., Su, Q., Horton, B. K., Bush, M. A., et al. (2019). Magnetic polarity stratigraphy, provenance, and paleoclimate analysis of Cenozoic strata in the Qaidam Basin, NE Tibetan Plateau. *GSA Bull.* 132, 310–320. doi:10.1130/B35175.1

Sun, Z., Yang, Z., Pei, J., Ge, X., Wang, X., Yang, T., et al. (2005). Magnetostratigraphy of Paleogene sediments from northern Qaidam Basin, China: implications for tectonic uplift and block rotation in northern Tibetan plateau. *Earth Planet. Sci. Lett.* 237, 635–646. doi:10.1016/j.epsl.2005.07.007

Suppe, J. (2007). Absolute fault and crustal strength from wedge tapers. *Geology* 35, 1127. doi:10.1130/G24053A.1

Wang, M., and Shen, Z. K. (2020). Present-day crustal deformation of continental china derived from GPS and its tectonic implications. *J. Geophys. Res. Solid Earth*, 125 (2), e2019JB018774. doi:10.1029/2019JB018774

Wang, E., Xu, F.-Y., Zhou, J.-X., Wang, S., Fan, C., and Wang, G. (2008). Vertical-axis bending of the Altyn Tagh belt along the Altyn Tagh fault: evidence from late cenozoic deformation within and around the xorkol basin. *Geol. Soc. America Spec. Paper* 444, 25–44. doi:10.1130/2008.2444(02

Wang, W., Zheng, W., Zhang, P., Li, Q., Kirby, E., Yuan, D., et al. (2017). Expansion of the Tibetan plateau during the neogene. *Nat. Commun.* 8, 15887. doi:10.1038/ncomms15887

Wei, Y., Xiao, A., Wu, L., Mao, L., Zhao, H., Shen, Y., et al. (2016). Temporal and spatial patterns of cenozoic deformation across the Qaidam Basin, northern Tibetan plateau. *Terra Nova* 28, 409–418. doi:10.1111/ter.12234

Wu, L., Lin, X., Cowgill, E., Xiao, A., Cheng, X., Chen, H., et al. (2019). Middle Miocene reorganization of the Altyn Tagh fault system, northern Tibetan plateau. *GSA Bull.* 131, 1157–1178. doi:10.1130/B31875.1

Wu, L., Xiao, A., Ma, D., Li, H., Xu, B., Shen, Y., et al. (2014). Cenozoic fault systems in southwest Qaidam Basin, northeastern Tibetan Plateau: geometry, temporal development, and significance for hydrocarbon accumulation. *Bulletin* 98, 1213–1234. doi:10.1306/11131313087

Xiao, A., Wu, L., Li, H., and Wang, L. (2013). Tectonic processes of the cenozoic Altyn Tagh fault and its coupling with the Qaidam Basin, NW China. *Acta Petrologica Sinica* 29, 2826–2836. [in Chinese with English abstract]

Yang, F., Sun, Z. C., Ma, Z. Q., and Zhang, Y. H. (1997). Quaternary ostrcode zones and magneto stratigraphic profile in the Qaidam Basin. *Acta Micropalaeontologica Sinica* 26-33, 35–38. [in Chinese with English abstract]

Yin, A., Rumelhart, P. E., Butler, R., Cowgill, E., Harrison, T. M., Foster, D. A., et al. (2002). Tectonic history of the Altyn Tagh fault system in northern Tibet inferred from Cenozoic sedimentation. *Geol. Soc. Am. Bull.* 114, 1257–1295. doi:10.1130/0016-7606(2002)114<1257:THOTAT>2.0.CO;2

Yu, X., Fu, S., Guan, S., Huang, B., Cheng, F., Cheng, X., et al. (2014). Paleomagnetism of Eocene and Miocene sediments from the Qaidam basin: implication for no integral rotation since the Eocene and a rigid Qaidam block. *Geochem. Geophys. Geosyst.* 15, 2109–2127. doi:10.1002/2014GC005230

Zhang, P. Z., Molnar, P., and Xu, X. (2007). Late quaternary and present-day rates of slip along the Altyn Tagh fault, northern margin of the Tibetan plateau. *Tectonics* 26, TC5010. doi:10.1029/2006tc002014

Zhang, W., Fang, X., Song, C., Appel, E., Yan, M., and Wang, Y. (2013). Late Neogene magnetostratigraphy in the western Qaidam Basin (NE Tibetan Plateau) and its constraints on active tectonic uplift and progressive evolution of growth strata. *Tectonophysics* 599, 107–116. doi:10.1016/j.tecto.2013.04.010

Zhao, H., Wei, Y., Shen, Y., Xiao, A., Mao, L., Wang, L., et al. (2016). Cenozoic tilting history of the south slope of the Altyn Tagh as revealed by seismic profiling: implications for the kinematics of the Altyn Tagh fault bounding the northern margin of the Tibetan Plateau. *Geosphere* 12, 884–899. doi:10.1130/GES01269.1

Zheng, W. J., Zhang, P. Z., He, W. G., Yuan, D. Y., Shao, Y. X., Zheng, D. W., et al. (2013). Transformation of displacement between strike-slip and crustal shortening in the northern margin of the Tibetan Plateau: evidence from decadal GPS measurements and late Quaternary slip rates on faults. *Tectonophysics* 584, 267–280. doi:10.1016/j.tecto.2012.01.006

Zhou, J., Xu, F., Wang, T., Cao, A., and Yin, C. (2006). Cenozoic deformation history of the Qaidam Basin, NW China: results from cross-section restoration and implications for Qinghai-Tibet Plateau tectonics. *Earth Planet. Sci. Lett.* 243, 195–210. doi:10.1016/j.epsl.2005.11.033

Zhu, L., Wang, C., Zheng, H., Xiang, F., Yi, H., and Liu, D. (2006). Tectonic and sedimentary evolution of basins in the northeast of Qinghai-Tibet Plateau and their implication for the northward growth of the Plateau. *Palaeogeogr. Palaeoclimatol. Palaeoecol.* 241, 49–60. doi:10.1016/j.palaeo.2006.06.019

Conflict of Interest: Author JZ is employed by Bureau of Geophysical Prospecting Inc. Authors YZ and YC are employed by Qinghai Oilfield Company, PetroChina. The remaining authors declare that the research was conducted in the absence of any commercial or financial relationships that could be construed as a potential conflict of interest.